Quantifying the Incoherent M_2 Internal Tide in the Philippine Sea

COLETTE G. KERRY,[a] BRIAN S. POWELL, AND GLENN S. CARTER

University of Hawai'i at Mānoa, Honolulu, Hawaii

(Manuscript received 22 January 2016, in final form 13 June 2016)

ABSTRACT

The baroclinic tides are a crucial source of mixing energy into the deep ocean; however, the incoherent portion of the spectrum is not well examined because it is difficult to observe. This study estimates the coherent and incoherent M_2 internal tide energy fluxes in the Philippine Sea using a primitive equation model that resolves the M_2 barotropic and baroclinic tides and the time-evolving atmospherically forced eddying circulation. A time-mean, incoherent, internal tide energy flux of 25% of the coherent energy flux is found to emanate eastward into the Philippine Sea from the Luzon Strait and a time-mean incoherent portion of 30% of the coherent energy flux propagates westward into the South China Sea (SCS). The incoherent internal tide energy results from baroclinic tide generation and propagation variability. Quantifying the incoherent portion estimates the energy missing from altimeter-derived or line-integral acoustic measurements and places short-lived, in situ observations in the context of variability.

1. Introduction

The time-variable (incoherent) portion of the internal tide is difficult to observe over large areas and may be a significant portion of the total, internal tide energy in some regions. Several studies have estimated the time-invariant internal tide using regional, ocean basin, and global-scale models (e.g., Niwa and Hibiya 2001; Merrifield and Holloway 2002; Niwa and Hibiya 2004; Simmons et al. 2004; Carter et al. 2008; Zilberman et al. 2009; Shriver et al. 2012; Kerry et al. 2013); satellite altimetry (Dushaw 2002; Ray and Zaron 2011; Zhao and D'Asaro 2011; Zhao 2014; Ray and Zaron 2016); and long-range acoustic transmissions (Dushaw et al. 1995). However, internal tide generation, propagation, and dissipation variability can be significant (Rainville and Pinkel 2006; Zaron et al. 2009; Chavanne et al. 2010a; Kelly and Nash 2010). Internal tide generation can vary because of changes to the stratification over an internal tide generation site and the phasing of remotely generated internal tides (Colosi and Munk 2006; Osborne et al. 2011; Kerry et al. 2013, 2014a), and the propagating internal tide can be modulated by the background circulation (e.g., Olbers 1981; van Haren 2004; Park and Watts 2006; Rainville and Pinkel 2006; Chavanne et al. 2010b; Zaron and Egbert 2014).

Observations capable of observing the internal tide over large areas include satellite altimetry and long-range acoustic measurements. With present altimeters, the observed tides are aliased into longer periods such that the internal tide signal detected by the altimeter is only the component that is phase locked with the tidal forcing and time invariant over the duration of the harmonic analysis (e.g., Ray and Zaron 2016). Likewise, acoustic travel times provide synoptic integrals of the ocean state along long-range transmissions and are only capable of detecting the phase-locked internal tide (Dushaw et al. 1995). Mooring-based observations can capture the temporal variability of internal tides and have shown highly variable baroclinic tides near the Hawaiian Ridge (Zilberman et al. 2011) and at the Luzon Strait (Pickering et al. 2015).

Quantifying internal tide incoherence is an important step toward understanding the predictability of internal tides. Predicting the propagation and dissipation of internal tide energy is key to closing the energy budget of the deep ocean, estimating the distribution of mixing, and developing subgrid-scale mixing parameterizations for

[a] Current affiliation: University of New South Wales, Sydney, New South Wales, Australia.

Corresponding author address: Colette Kerry, School of Mathematics and Statistics, University of New South Wales, Sydney, NSW 2052, Australia.
E-mail: c.kerry@unsw.edu.au

DOI: 10.1175/JPO-D-16-0023.1

global ocean circulation models used in climate simulations (e.g., Jayne 2009). Furthermore, internal tide prediction will be of particular interest for the wide-swath altimeter mission planned for the near-future (Fu and Ubermann 2014), which will require that the internal tide be removed in order to study ocean submesoscale variability.

The Luzon Strait is the generation site of some of the strongest internal tides observed worldwide (Ramp et al. 2004; Alford et al. 2011, 2015), which propagate westward into the South China Sea (SCS) and eastward into the Philippine Sea and have been shown to be highly variable (Kerry et al. 2014a; Shriver et al. 2014). This paper uses a model that includes the M_2 internal tides and the time-evolving atmospherically forced circulation to quantitatively estimate the time-invariant (coherent) portion of the energy that propagates away from the generation site and the time-variable (incoherent) portion.

2. Model description

This study is based on a Regional Ocean Modeling System (ROMS) configuration that simulates the eddying general circulation and the principal lunar, semidiurnal M_2 barotropic and baroclinic tides in the Philippine Sea. This same model was used in Kerry et al. (2014a,b) and the configuration is described in detail in those publications where it is referred to as the Full case. ROMS solves the free-surface, primitive equations on a curvilinear grid with a terrain-following vertical coordinate system, making the hydrostatic and Boussinesq approximations. Shchepetkin and McWilliams (1998, 2003, 2005) provide detailed description of the ROMS computational kernel. We focus on internal tide propagation into deep water, into the Philippine Sea, and into the SCS prior to interaction with the shelf; such that the hydrostatic approximation remains valid as the internal tide horizontal wavelengths are much greater than the associated scales of vertical displacement.

The model domain is bounded between 116.9° and 136.9°E and 15.9° and 24.9°N, encompassing the Luzon Strait and extending from the SCS in the west to the central Philippine Sea in the east (refer to Fig. 1). The grid has a horizontal resolution of 8 km over most of the domain, with a higher zonal resolution of 4.5 km over the Luzon Strait to improve bathymetric resolution and minimize horizontal pressure gradient errors over the steep topography. In the vertical, 25 *s*-coordinate layers are distributed with a higher resolution in the upper 250 m. The model is nested within a larger domain that encompasses the entire Philippine Sea including both the Luzon Strait and the Mariana Island Arc internal tide generation sites. This ensures that the influence of the internal tides generated at the Mariana Arc under the varying subtidal dynamics is included, as was shown to be important in Kerry et al. (2013, 2014a). The simulation is integrated for the year 2010 with a 1-month spinup period.

The major subtidal circulation features are well represented in the model, including the intrusion of the Kuroshio into the Luzon Strait (the Loop Current), the northward-flowing Kuroshio along the east coast of Taiwan and the location of the Subtropical Front, the North Equatorial Current (NEC) and the Subtropical Countercurrent in the mean flow. The model provides a comparable representation of the low-frequency variability in the SSH associated with the mesoscale field compared with AVISO observations. The variability of internal tides in the presence of varying subtidal circulation is well represented in the model when compared with observations from a Deep-Ocean Assessment and Reporting of Tsunamis (DART) buoy in the central Philippine Sea. More details on the comparisons of the modeled mean flow and variability with available observations can be found in Kerry et al. (2014a). The simulated internal tide energy fluxes are compared to observations of baroclinic energy fluxes at the Luzon Strait (Alford et al. 2011) in section 4 of Kerry et al. (2014a). The modeled semidiurnal (combined M_2 and S_2) fluxes show significant variability in both flux magnitude and direction, and the modeled standard deviation ellipses mostly contain the briefly observed fluxes.

3. Results and discussion

Energy from the barotropic tide is converted into baroclinic tidal energy at the two parallel, north–south-orientated steep ridges of the Luzon Strait. Baroclinic internal tide generation at the Luzon Strait ranges from a minimum of 13.01 GW to a maximum of 19.95 GW, with the time-mean generation of 16.21 GW over the year-long 2010 simulation (Kerry et al. 2014a). This energy propagates westward into the SCS and eastward in the Philippine Sea as internal tides. The depth-integrated baroclinic tidal flux is given by the time-averaged product of the pressure and velocity perturbations over a number of tidal cycles,

$$\mathbf{F}_{\mathrm{bc}} = \frac{1}{T_\theta}\int_0^{T_\theta}\int_{-H}^{\eta} \mathbf{u}'_\theta(z,t)p'_\theta(z,t)\,dz\,dt, \qquad (1)$$

and represents the radiation of internal tide energy. The pressure perturbation is given by $p'_\theta(z,t) = p_\theta(z,t) - \overline{p}_\theta(z) - \overline{p}_0(t)$, where $\overline{p}_\theta(z)$ is the time-mean quantity, and $\overline{p}_0(t) = [1/(H+\eta_\theta)]\int_{-H}^{\eta_\theta}[p_\theta(z,t) - \overline{p}_\theta(z)]\,dz$ ensures the

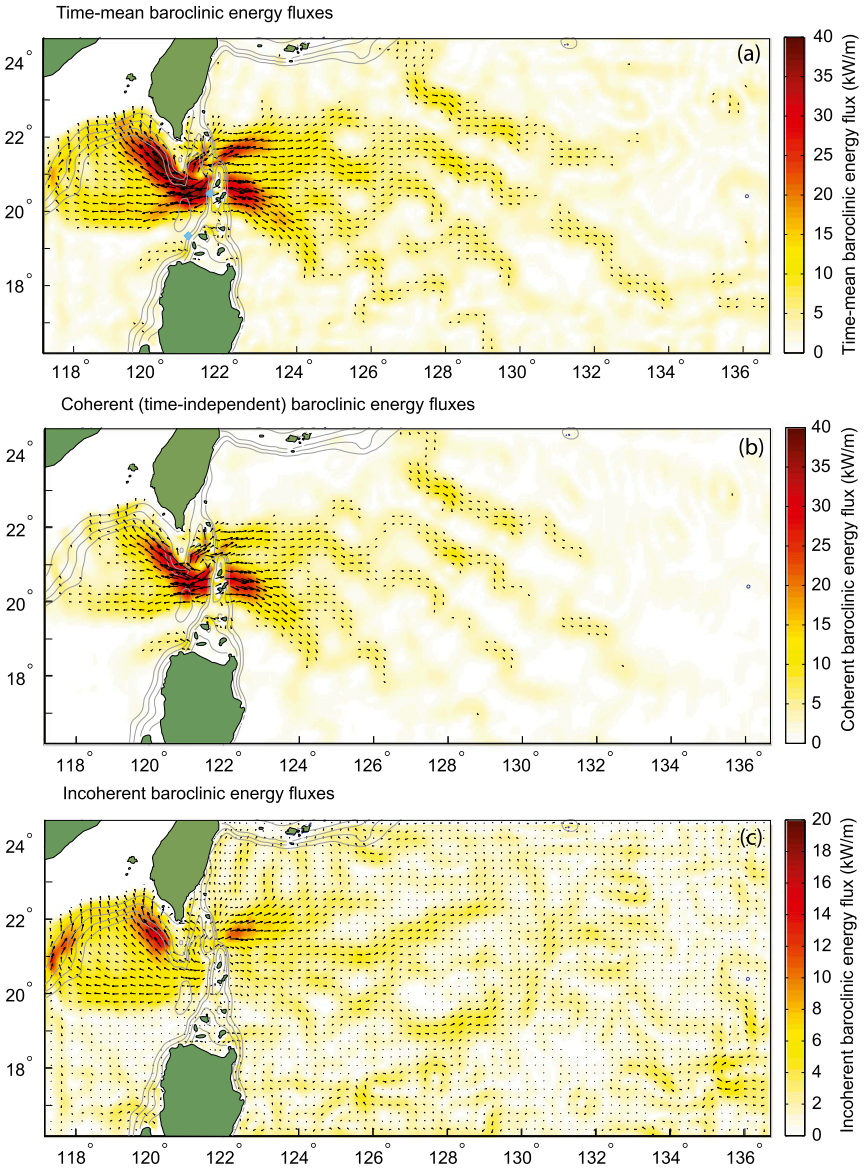

FIG. 1. Depth-integrated M_2 baroclinic energy fluxes over the model domain: (a) time mean, (b) coherent, and (c) incoherent (given by the time mean of total minus coherent fluxes). Note the change in scale for the bottom panel. The blue diamonds in the top panel show the locations of the moorings from Pickering et al. (2015); A1 (central Luzon Strait) and S9 (southwestern Luzon Strait).

baroclinicity condition is satisfied. The velocity perturbation is given by $\mathbf{u}'_\theta(z, t) = \mathbf{u}_\theta(z, t) - \overline{\mathbf{u}}_\theta(z) - \overline{\mathbf{u}}_0(t)$, where $\overline{\mathbf{u}}_\theta(z)$ is the time-mean quantity and, by the baroclinicity condition, $\overline{\mathbf{u}}_0(t) = [1/(H + \eta_\theta)]\int_{-H}^{\eta_\theta}[\mathbf{u}_\theta(z, t) - \overline{\mathbf{u}}_\theta(z)]\,dz$. We compute the energy fluxes using tidal harmonic components to avoid undersampling of the tidal amplitudes.

The horizontal propagation of the depth-integrated baroclinic energy fluxes varies in time and space in the presence of the varying subtidal circulation, resulting in incoherent internal tide signals. The coherent portion of the internal tide is defined here as the phase-locked, time-independent internal tide, and the incoherent tide is the time-variable portion. The coherent portion is calculated from the harmonic analysis of the entire year-long time series. To estimate the time-variant incoherent portion we compute the depth-integrated baroclinic energy fluxes every 3 days over the year-long model simulation. The 3-day windows are chosen as the background mesoscale field varies little over this

time period, and this time period encompasses 5 full M_2 tidal cycles for harmonic analysis. The time mean of the three daily baroclinic energy fluxes are shown in Fig. 1a, and the coherent baroclinic energy fluxes in Fig. 1b (the flux vectors are plotted every three model grid points with only flux magnitude values greater than $4\,\mathrm{kW\,m^{-1}}$ shown). The incoherent portion of the baroclinic energy fluxes is defined as the difference between the total baroclinic energy fluxes calculated every 3 days and the coherent baroclinic energy fluxes. The time-mean incoherent portion is shown in Fig. 1c.

Of the eastward fluxes emanating from the Luzon Strait, the southeastward beam remains largely coherent, with coherent fluxes up to $30\,\mathrm{kW\,m^{-1}}$ compared to a small incoherent component (fluxes $< 5\,\mathrm{kW\,m^{-1}}$). The time-mean incoherent flux magnitudes are 5%–20% of the coherent flux magnitudes in this beam. The northeastward beam has a greater incoherent portion, with time-mean incoherent fluxes peaking at $12\,\mathrm{kW\,m^{-1}}$, compared to a maximum coherent flux magnitude of approximately $20\,\mathrm{kW\,m^{-1}}$ in this beam. Time-mean incoherent flux magnitudes are 60%–80% of the coherent magnitudes over the beam. The fluxes in the northeastward beam originate from both the northern region of the eastern slope of the eastern ridge and the eastern slope of the western ridge [refer to Fig. 1a and also found by Jan et al. (2008)]. Generation variability is particularly large over the northern region of the eastern slope of the eastern ridge. Kerry et al. (2014a) show that the standard deviation in barotropic to baroclinic conversion is greater than the time-mean conversion here. This is the only significant internal tide generation site in the Luzon Strait where this is the case. The generation variability results predominantly from changes in the phase difference between the pressure perturbation and the vertical barotropic velocity at the bottom and, to a lesser extent, changes in the bottom pressure perturbation amplitude. This implies that the generation variability stems from variable remotely generated internal tides traveling long distances through changing background circulation and stratification rather than local stratification changes that influence the pressure perturbation amplitude. As the northeastern beam propagates away from the generation sites into the deep Philippine Sea, the coherent flux magnitude decreases and the incoherent flux increases. This increase in incoherence is likely to result from modulation of the propagating internal tide in the region of high EKE where the Kuroshio intrusion (Loop Current) exits the Luzon Strait [as shown in Fig. 5c of Kerry et al. (2014a)]. The dominance of the incoherent portion in the northeastward beam is consistent with Zhao (2014), who finds that the M_2 internal tides here are undetectable to the satellite altimeters within three wavelengths of the Luzon Strait, while the southeastward beam detected by the altimeter data propagates over 1000 km.

A significant portion of the total M_2 internal tide energy in the SCS is incoherent. The incoherent fluxes are strongest in magnitude in the region directly west of the northern portion of the western ridge, where the fluxes are directed northwestward parallel to the continental slope. The time-mean incoherent fluxes here peak at $15\,\mathrm{kW\,m^{-1}}$ compared to coherent flux magnitudes that reach $30\,\mathrm{kW\,m^{-1}}$. The fluxes emanating westward from the middle portion of the Luzon Strait have a time-mean, incoherent portion of about 70% of the coherent portion, with coherent fluxes of about $12\,\mathrm{kW\,m^{-1}}$ in this beam and incoherent flux magnitudes of $8\,\mathrm{kW\,m^{-1}}$. The westward-propagating internal tides are generated both on the western slope of the eastern ridge and on the western ridge (Chao et al. 2007; Jan et al. 2008; Kerry et al. 2013). Chao et al. (2007) show that the western ridge in the middle portion of the Luzon Strait dampens the M_2 internal tides from the eastern ridge, while the northern part of the western ridge is a secondary generation site reinforcing the westward-propagating M_2 baroclinic tides. The westward-shoaling stratification of the Kuroshio is predicted to enhance the amplitude of the internal tides propagating into the SCS (Buijsman et al. 2010b), resulting in variable amplitude depending on the extent of the Loop Current into the Luzon Strait. Furthermore, Buijsman et al. (2010a) suggest amplification of the westward-propagating internal tides results from resonant interactions between internal tides generated at both ridges. The strength of the resonant response depends on the background stratification and is thus likely to be temporally variant. The Loop Current has been shown to have a steering effect (Kerry et al. 2013, 2014a), and its significant spatial variability (Yuan et al. 2006; Nan et al. 2011; Rudnick et al. 2011) will cause incoherence of the propagating internal tides due to time-variable refraction. This process was shown to result in an incoherent flux of about 20% of the coherent flux emanating from the Hawaiian Ridge (Zaron and Egbert 2014). The zonal component of the background current associated with the Loop Current can also alter the phase of the westward-propagating internal tides by a Doppler shifting effect (Li and Farmer 2011).

The internal tides in the SCS steepen and become highly nonlinear and nonhydrostatic as they interact with the continental shelf to the west (Alford et al. 2010; Farmer et al. 2011). The ROMS model handles nonlinear processes but makes the hydrostatic approximation and is not expected to correctly represent the internal tides as they shoal in the western SCS.

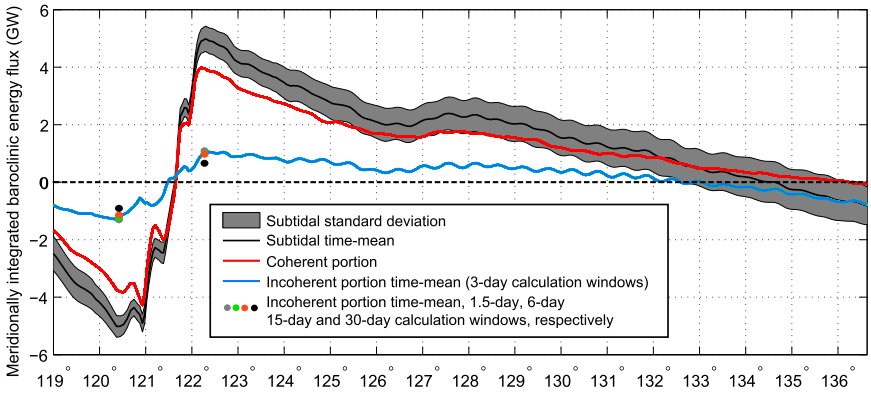

FIG. 2. Meridionally and depth-integrated M_2 baroclinic energy fluxes across model domain. The subtidal time-mean and incoherent portion time-mean are computed using 3-day windows. The incoherent portion time means at 120.4° and 122.3°E computed using four different window sizes are shown by the dots.

Estimation of the shoaling process is outside of the scope of this study, and the magnitude of the incoherent fluxes over the continental slope at the western edge of the domain, between 20° and 22°N, is ignored in this analysis.

Integrating the depth-integrated baroclinic energy fluxes meridionally across the domain illustrates the decay of the energy fluxes as they propagate eastward and westward away from the principal generation site at the Luzon Strait (Fig. 2). The black line represents the time mean of the three daily baroclinic energy fluxes, and the gray shaded area shows the standard deviation about the mean. Variability of the incoherent flux increases with distance from the generation site. The coherent portion (red line) peaks at 4.0 GW eastward at 122.3°E, 80% of the total time-mean eastward peak of 5.0 GW, and at 4.3 GW westward at 120.4°E, 86% of the 5.0-GW, total, time-mean westward peak. The time-averaged, incoherent, energy flux (blue line) peaks at 1.0 GW eastward and 1.3 GW westward into the Philippine Sea and the SCS, respectively. This represents an incoherent portion of 25% of the coherent flux into the Philippine Sea and of 30% into the SCS. These percentages correspond to the longitudes where the meridionally integrated eastward and westward baroclinic energy fluxes have the greatest magnitude, at 122.3° and 120.4°E, respectively.

Close to the generation site, the incoherence results from generation variability. As we move away from the main generation region (121°–122°E) to the west, the incoherent portion as a percentage of the coherent portion (not shown) increases from 15% at 121°E to 50% at 118.5°E before beginning to decrease to the west. For the eastward-propagating fluxes, the incoherent percentage increases from 16% at 122°E to 37% at 125°E before beginning to decrease to the east. This indicates that the modulation of the propagating internal tide results in increased incoherence with distance from the generation site, consistent with findings by Pickering et al. (2015). In Kerry et al. (2013), the mode-2 internal tide represents a constant percentage of the total eastward meridionally integrated baroclinic energy flux emanating from the Luzon Strait until 125°E, east of which the percentage begins to decay, reaching zero at 137°E. The percentage of internal tide energy represented by mode 3 decays to zero from the generation site to 125°E. The increased dominance of mode-1 energy east of 125°E in Kerry et al. (2013) corresponds to the decrease in the ratio of incoherent to coherent internal tide energy found in this study. This suggests that the increased incoherence with distance from the generation site to 125°E results from higher-mode, internal tide energy that is more influenced by propagation effects, while the mode-1 internal tide propagates further and remains coherent over a greater distance. The propagation speed decreases and, as shown by Rainville and Pinkel (2006), the effect of the mesoscale currents on refraction and Doppler shifting increases with the mode number. It should be noted that Kerry et al. (2013) does not include the atmospherically forced eddying circulation, so the decay of the higher modes is expected to be faster in this study.

An increase in both the coherent and incoherent portions of the eastward flux is seen between 127° and 128°E because of the internal tides generated at the Ryukyu Ridge (located to the east of Taiwan in the northern portion of the model domain). Internal tide generation at the Ryukyu Ridge can be seen in Fig. 5 of Kerry et al. (2013), and in Kerry et al. (2014b), a

peak in internal tide dissipation was found at 128°E, associated with the internal tides from this generation site. The coherent portion of the internal tide energy flux in the Philippine Sea remains eastward across the entire domain (Fig. 2), while the incoherent portion becomes dominated by westward fluxes from the Mariana Arc east of 132°E (Fig. 2), as the low-mode internal tides propagate further and are expected to remain coherent over longer distances.

Pickering et al. (2015) compute internal tide incoherence at two mooring sites in the Luzon Strait with full-depth coverage over 50 days: one on the eastern ridge in central Luzon Strait (A1) and one on the southwestern side of the eastern ridge in the southern Luzon Strait (S9; locations shown on Fig. 1a). They estimate the coherence of the baroclinic energy fluxes as the percent of variance that is explained by the harmonic fit of the signal over the 50-day data record. For the semidiurnal band, they find an incoherent portion of 17% for A1 and 25% for S9 (refer to their Fig. 15). These values are smaller than the time-averaged incoherent portions found in this study at 122.3° (25%) and 120.4°E (30%). Their measurements are closer to the internal tide generation site, whereas at 122.3° and 120.4°E the fluxes may experience greater variability as they propagate away from the generation region. Furthermore, our calculations are performed over 1 yr, so we would expect higher incoherence compared to calculations based on a 50-day record. Zaron and Egbert (2014) estimate a 20% incoherent portion for the Hawaiian Ridge at a distance of 250 km from the ridge axis; however, they note that this is likely to be an underestimate due to the relatively smooth background fields through which they propagate the internal tides. The Hawaiian region also has lower eddy kinetic energy compared to the Luzon region (Jia et al. 2011).

Calculations to compute the time-varying internal tide energy fluxes were also performed using 1.5-, 6-, 15-, and 30-day windows, and the resulting time-mean incoherent portions of the meridionally integrated baroclinic energy flux at 120.4° and 122.3°E are shown by the dots on Fig. 2. At 120.4°E, the magnitude of the time-mean incoherent flux is 1.9% greater using 1.5-day windows, compared to 3-day windows, and 3.3%, 10.7%, and 29.0% smaller using 6-, 15-, and 30-day windows, respectively. At 122.3°E, the magnitude of the time-mean incoherent flux is 3.0% greater using 1.5-day windows, compared to 3-day windows, and 7.0%, 8.1%, and 37.9% smaller using 6-, 15-, and 30-day windows, respectively. This indicates that a considerable amount of the internal tide variability occurs over time scales less than 15 to 30 days and, as only a small amount of the additional variability is captured using 1.5-day windows, that internal tides vary little over periods less than 3 days. As such, we consider the 3-day window used in this study to be a good choice for estimation of the incoherent internal tide energy fluxes.

To examine the temporal variability of the eastward and westward fluxes from the Luzon Strait, the time series of the meridionally integrated internal tide energy fluxes are shown through 122.3°E in Fig. 3a and through 120.4°E in Fig. 3c. The incoherent flux as a percentage of the coherent flux propagating eastward into the Philippine Sea (Fig. 3b) varies from a negative value (the incoherent fluxes are westward) to 72% over the year, with a time mean of 25%. Fluxes propagating westward into the SCS have an incoherent portion that reaches 76% of the meridionally integrated coherent flux magnitude (Fig. 3d), with a time mean of 30%.

4. Conclusions

Estimating the propagation of internal tides is important in predicting where the transfer of energy to smaller scales and dissipation ultimately occurs. While the coherent (phase locked, time invariant) portion can be observed from altimeter data, the incoherent portion is largely unknown. This study provides a quantitative estimate of the incoherent M_2 internal tide in the Philippine Sea, a region of significance to the global internal tide energy budget. We estimate time-mean, meridionally integrated, incoherent fluxes of 25% of the coherent flux emanating eastward into the Philippine Sea from the Luzon Strait, and a time-mean incoherent portion of 30% of the coherent, meridionally integrated fluxes propagating westward into the SCS. These percentages correspond to the longitudes of peak eastward and westward meridionally integrated flux magnitudes.

Incoherent internal tide signals result from variability in both the generation and propagation of the baroclinic tides. We hypothesize that the highly variable nature of the Loop Current is responsible for the significant incoherent portion of the M_2 internal tide in the SCS. Two distinct eastward beams propagating into the Philippine Sea are evident in the time-mean baroclinic energy fluxes. We find that the southeastward beam has a dominant coherent portion, while the northeastward beam has a greater incoherent portion. We hypothesize that the high incoherence in the northeastward beam is related to increased generation variability predominately caused by variable, remotely generated internal tides, rather than local stratification changes, and modulation of the propagating internal tide in the region of high EKE where the Loop Current leaves the Luzon Strait.

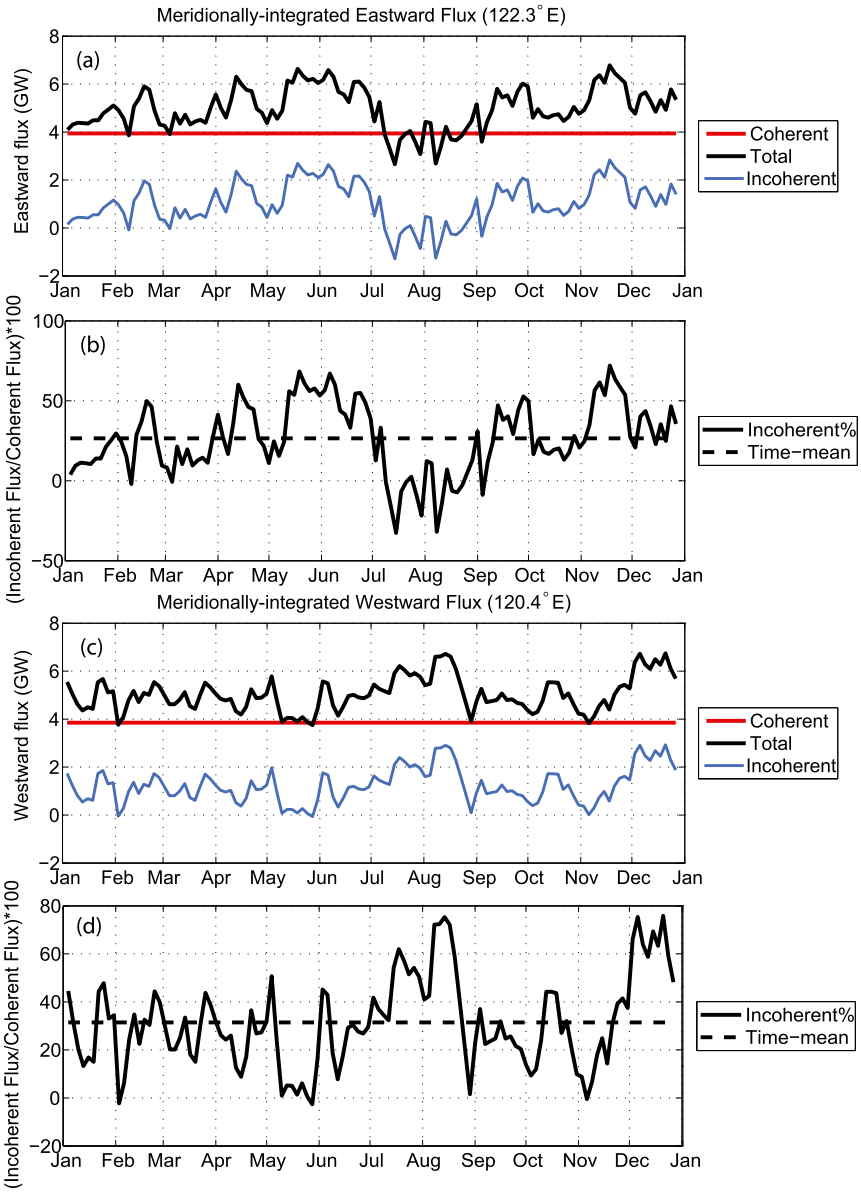

FIG. 3. (a) Time series of meridionally and depth-integrated M_2 baroclinic energy fluxes through 122.3°E and (b) corresponding incoherent flux as a percentage of the coherent flux. (c) Time series of meridionally and depth-integrated M_2 baroclinic energy fluxes through 120.4°E and (d) corresponding incoherent flux as a percentage of the coherent flux. Note that eastward fluxes are positive in (a) and westward fluxes are positive in (c).

The model estimates of the incoherent portion of the internal tide presented here are expected to represent a lower bound as some of the processes that cause scattering of the coherent tide are not resolved, such as nonlinear interactions of multiple tidal frequencies and interaction with submesoscale features. Furthermore, as harmonic fits to satellite data have to be over periods longer than a year, these estimates for a 1-yr modeled time period are likely to result in a lower incoherent proportion. This study has only considered the M_2 internal tide. Pickering et al. (2015) found significant differences in the incoherent portion for diurnal and semidiurnal tides at a mooring located on the eastern ridge and further modeling work could consider more tidal constituents.

Acknowledgments. Dr. Kerry and Dr. Powell were supported by ONR Grant N00014-13-1-0514 and Dr. Carter was supported by ONR Grant N00014-10-1-0334. We thank Dr. Thomas Decloedt, previously of the

Department of Oceanography at the University of Hawaii, for his useful discussions.

REFERENCES

Alford, M. H., R.-C. Lien, H. Simmons, J. Klymak, S. Ramp, Y. J. Yang, D. Tang, and M.-H. Chang, 2010: Speed and evolution of nonlinear internal waves transiting the South China Sea. *J. Phys. Oceanogr.*, **40**, 1338–1355, doi:10.1175/2010JPO4388.1.

——, and Coauthors, 2011: Energy flux and dissipation in Luzon Strait: Two tales of two ridges. *J. Phys. Oceanogr.*, **41**, 2211–2222, doi:10.1175/JPO-D-11-073.1.

——, and Coauthors, 2015: The formation and fate of internal waves in the South China Sea. *Nature*, **521**, 65–69, doi:10.1038/nature14399.

Buijsman, M. C., Y. Kanarska, and J. C. McWilliams, 2010a: On the generation and evolution of nonlinear internal waves in the South China Sea. *J. Geophys. Res.*, **115**, C02012, doi:10.1029/2009JC005275.

——, J. C. McWilliams, and C. R. Jackson, 2010b: East-west asymmetry in nonlinear internal waves from Luzon Strait. *J. Geophys. Res.*, **115**, C10057, doi:10.1029/2009JC006004.

Carter, G. S., and Coauthors, 2008: Energetics of M_2 barotropic-to-baroclinic tidal conversion at the Hawaiian Islands. *J. Phys. Oceanogr.*, **38**, 2205–2223, doi:10.1175/2008JPO3860.1.

Chao, S. Y., D. S. Ko, R. C. Lien, and P. T. Shaw, 2007: Assessing the west ridge of Luzon Strait as an internal wave mediator. *J. Oceanogr.*, **63**, 897–911, doi:10.1007/s10872-007-0076-8.

Chavanne, C., P. Flament, G. Carter, M. Merrifield, and D. Luther, 2010a: The surface expression of semidiurnal internal tides near a strong source at Hawaii. Part I: Observations and numerical predictions. *J. Phys. Oceanogr.*, **40**, 1155–1179, doi:10.1175/2010JPO4222.1.

——, ——, and D. Luther, 2010b: The surface expression of semidiurnal internal tides near a strong source at Hawaii. Part II: Interactions with mesoscale currents. *J. Phys. Oceanogr.*, **40**, 1180–1200, doi:10.1175/2010JPO4223.1.

Colosi, J. A., and W. Munk, 2006: Tales of the venerable Honolulu tide gauge. *J. Phys. Oceanogr.*, **36**, 967–996, doi:10.1175/JPO2876.1.

Dushaw, B. D., 2002: Mapping low-mode internal tides near Hawaii using TOPEX/POSEIDON altimeter data. *Geophys. Res. Lett.*, **29**, 91-1–91-4, doi:10.1029/2001GL013944.

——, B. D. Cornuelle, P. F. Worcester, B. M. Howe, and D. S. Luther, 1995: Barotropic and baroclinic tides in the central North Pacific Ocean determined from long-range reciprocal acoustic transmissions. *J. Phys. Oceanogr.*, **25**, 631–647, doi:10.1175/1520-0485(1995)025<0631:BABTIT>2.0.CO;2.

Farmer, D. M., M. H. Alford, R.-C. Lien, Y. J. Yang, M.-H. Chang, and Q. Li, 2011: From Luzon to Dongsha Plateau: Stages in the life of an internal wave. *Oceanography*, **24**, 64–77, doi:10.5670/oceanog.2011.95.

Fu, L. L., and C. Ubermann, 2014: On the transition from profile altimeter to swath altimeter for observing global ocean surface topography. *J. Atmos. Oceanic Technol.*, **31**, 560–568, doi:10.1175/JTECH-D-13-00109.1.

Jan, S., R.-C. Lien, and C.-H. Ting, 2008: Numerical study of baroclinic tides in Luzon Strait. *J. Oceanogr.*, **64**, 789–802, doi:10.1007/s10872-008-0066-5.

Jayne, S. R., 2009: The impact of abyssal mixing parameterizations in an ocean general circulation model. *J. Phys. Oceanogr.*, **39**, 1756–1775, doi:10.1175/2009JPO4085.1.

Jia, F., L. Wu, and B. Qiu, 2011: Seasonal modulation of eddy kinetic energy and its formation mechanism in the southeast Indian Ocean. *J. Phys. Oceanogr.*, **41**, 657–665, doi:10.1175/2010JPO4436.1.

Kelly, S. M., and J. D. Nash, 2010: Internal-tide generation and destruction by shoaling internal tides. *Geophys. Res. Lett.*, **37**, L23611, doi:10.1029/2010GL045598.

Kerry, C. G., B. S. Powell, and G. S. Carter, 2013: Effects of remote generation sites on model estimates of M_2 internal tides in the Philippine Sea. *J. Phys. Oceanogr.*, **43**, 187–204, doi:10.1175/JPO-D-12-081.1.

——, ——, and ——, 2014a: The impact of subtidal circulation on internal tide generation and propagation in the Philippine Sea. *J. Phys. Oceanogr.*, **44**, 1386–1405, doi:10.1175/JPO-D-13-0142.1.

——, ——, and ——, 2014b: The impact of subtidal circulation on internal-tide-induced mixing in the Philippine Sea. *J. Phys. Oceanogr.*, **44**, 3209–3224, doi:10.1175/JPO-D-13-0249.1.

Li, Q., and D. M. Farmer, 2011: The generation and evolution of nonlinear internal waves in the deep basin of the South China Sea. *J. Phys. Oceanogr.*, **41**, 1345–1363, doi:10.1175/2011JPO4587.1.

Merrifield, M. A., and P. E. Holloway, 2002: Model estimates of M_2 internal tide energetics at the Hawaiian Ridge. *J. Geophys. Res.*, **107**, 5-1–5-12, doi:10.1029/2001JC000996.

Nan, F., H. Xue, F. Chai, L. Shi, M. Shi, and P. Guo, 2011: Identification of different types of Kuroshio intrusion into the South China Sea. *Ocean Dyn.*, **61**, 1291–1304, doi:10.1007/s10236-011-0426-3.

Niwa, Y., and T. Hibiya, 2001: Numerical study of the spatial distribution of the M_2 internal tide in the Pacific Ocean. *J. Geophys. Res.*, **106**, 22 441–22 449, doi:10.1029/2000JC000770.

——, and ——, 2004: Three-dimensional numerical simulation of M_2 internal tides in the East China Sea. *J. Geophys. Res.*, **109**, C04027, doi:10.1029/2003JC001923.

Olbers, D. J., 1981: The propagation of internal waves in a geostrophic current. *J. Phys. Oceanogr.*, **11**, 1224–1233, doi:10.1175/1520-0485(1981)011<1224:TPOIWI>2.0.CO;2.

Osborne, J. J., A. L. Kurapov, G. D. Egbert, and P. M. Korso, 2011: Spatial and temporal variability of the M_2 internal tide generation and propagation on the Oregon shelf. *J. Phys. Oceanogr.*, **41**, 2037–2062, doi:10.1175/JPO-D-11-02.1.

Park, J.-H., and D. R. Watts, 2006: Internal tides in the southwestern Japan/East Sea. *J. Phys. Oceanogr.*, **36**, 22–34, doi:10.1175/JPO2846.1.

Pickering, A., M. Alford, J. Nash, L. Rainville, M. Buijsman, D. S. Ko, and B. Lim, 2015: Structure and variability of internal tides in Luzon Strait. *J. Phys. Oceanogr.*, **45**, 1574–1594, doi:10.1175/JPO-D-14-0250.1.

Rainville, L., and R. Pinkel, 2006: Propagation of low-mode internal waves through the ocean. *J. Phys. Oceanogr.*, **36**, 1220–1236, doi:10.1175/JPO2889.1.

Ramp, S. R., and Coauthors, 2004: Internal solitons in the northeastern South China Sea. Part I: Sources and deep water propagation. *IEEE J. Ocean. Eng.*, **29**, 1157–1181, doi:10.1109/JOE.2004.840839.

Ray, R. D., and E. D. Zaron, 2011: Non-stationary internal tides observed with satellite altimetry. *Geophys. Res. Lett.*, **38**, L17609, doi:10.1029/2011GL048617.

——, and ——, 2016: M_2 internal tides and their observed wavenumber spectra from satellite altimetry. *J. Phys. Oceanogr.*, **46**, 3–22, doi:10.1175/JPO-D-15-0065.1.

Rudnick, D. L., and Coauthors, 2011: Seasonal and mesoscale variability of the Kuroshio near its origin. *Oceanography*, **24**, 52–63, doi:10.5670/oceanog.2011.94.

Shchepetkin, A. F., and J. C. McWilliams, 1998: Quasi-monotone advection schemes based on explicit locally adaptive dissipation. *Mon. Wea. Rev.*, **126**, 1541–1580, doi:10.1175/1520-0493(1998)126<1541:QMASBO>2.0.CO;2.

——, and ——, 2003: A method for computing horizontal pressure-gradient force in an oceanic model with a nonaligned vertical coordinate. *J. Geophys. Res.*, **108**, 3090, doi:10.1029/2001JC001047.

——, and ——, 2005: The Regional Oceanic Modeling System (ROMS): A split-explicit, free-surface, topography-following-coordinate oceanic model. *Ocean Modell.*, **9**, 347–404, doi:10.1016/j.ocemod.2004.08.002.

Shriver, J. F., B. K. Arbic, J. G. Richman, R. D. Ray, E. J. Metzger, A. J. Wallcraft, and P. G. Timko, 2012: An evaluation of the barotropic and internal tides in a high-resolution global ocean circulation model. *J. Geophys. Res.*, **117**, C10024, doi:10.1029/2012JC008170.

——, J. G. Richman, and B. K. Arbic, 2014: How stationary are the internal tides in a high-resolution global ocean circulation model? *J. Geophys. Res. Oceans*, **119**, 2769–2787, doi:10.1002/2013JC009423.

Simmons, H. L., R. W. Hallberg, and B. K. Arbic, 2004: Internal wave generation in a global baroclinic tide model. *Deep-Sea Res. II*, **51**, 3043–3068, doi:10.1016/j.dsr2.2004.09.015.

van Haren, H., 2004: Some observations of nonlinearly modified internal wave spectra. *J. Geophys. Res.*, **109**, C03045, doi:10.1029/2003JC002136.

Yuan, D., W. Han, and D. Hu, 2006: Surface Kuroshio path in the Luzon Strait area derived from satellite remote sensing data. *J. Geophys. Res.*, **111**, C11007, doi:10.1029/2005JC003412.

Zaron, E. D., and G. D. Egbert, 2014: Time-variable refraction of the internal tide at the Hawaiian Ridge. *J. Phys. Oceanogr.*, **44**, 538–557, doi:10.1175/JPO-D-12-0238.1.

——, C. Chavanne, G. D. Egbert, and P. Flament, 2009: Baroclinic tidal generation in the Kauai Channel inferred from high-frequency radio Doppler current meters. *Dyn. Atmos. Oceans*, **48**, 93–120, doi:10.1016/j.dynatmoce.2009.03.002.

Zhao, Z., 2014: Internal tide radiation from the Luzon Strait. *J. Geophys. Res. Oceans*, **119**, 5434–5448, doi:10.1002/2014JC010014.

——, and E. D'Asaro, 2011: A perfect focus of the internal tide from the Mariana Arc. *Geophys. Res. Lett.*, **38**, L14609, doi:10.1029/2011GL047909.

Zilberman, N. V., J. M. Becker, M. A. Merrifield, and G. S. Carter, 2009: Model estimates of M_2 internal tide generation over Mid-Atlantic Ridge topography. *J. Phys. Oceanogr.*, **39**, 2635–2651, doi:10.1175/2008JPO4136.1.

——, M. A. Merrifield, G. S. Carter, D. S. Luther, M. D. Levine, and T. J. Boyd, 2011: Incoherent nature of M2 internal tides at the Hawaiian Ridge. *J. Phys. Oceanogr.*, **41**, 2021–2036, doi:10.1175/JPO-D-10-05009.1.